

Longitudinal diffusion tensor and manganese-enhanced MRI detect delayed cerebral gray and white matter injury after hypoxia–ischemia and hyperoxia

Tora Sund Morken¹, Marius Widerøe¹, Christina Vogt¹, Stian Lydersen², Marianne Havnes³, Jon Skranes¹, Pål Erik Goa⁴ and Ann-Mari Brubakk^{1,5}

BACKGROUND: Hypoxia–ischemia (HI) induces delayed inflammation and long-term gray and white matter brain injury that may be altered by hyperoxia.

METHODS: HI and 2 h of hyperoxia (100% O₂) or room air (21% O₂) in 7-d-old (P7) rats were studied by magnetic resonance imaging at 7 Tesla during 42 d: apparent diffusion coefficient (ADC) maps on day 1; T₁-weighted manganese-enhanced images on day 7; diffusion tensor images on days 21 and 42; and T₂ maps at all time points.

RESULTS: The long-term brain tissue destruction on T₂ maps was more severe in HI+hyperoxia than HI+room air. ADC was lower in HI+hyperoxia vs. HI+room air and sham and was correlated with long-term outcome. Manganese enhancement indicating inflammation was seen in both the groups along with more microglial activation in HI+hyperoxia on day 7. Fractional anisotropy (FA) in corpus callosum was lower and radial diffusivity was higher in HI+hyperoxia than that in HI+room air and sham on day 21. From day 21 to day 42, FA and radial diffusivity in HI+hyperoxia were unchanged, whereas in HI+room air, FA increased and radial diffusivity decreased to values similar to sham.

CONCLUSION: Hyperoxia caused a more severe tissue destruction, delayed irreversible white matter injury, and increased inflammatory response resulting in a worsening in the trajectory of injury after HI in developing gray and white matter.

Perinatal brain injury is a severe and often fatal condition that may lead to lifelong disabilities in survivors. Improved neonatal intensive care has led to increasing survival rates over the last decades, but disability rates have not improved correspondingly, in part due to the increasing number of preterm born infants who survive (1). The ensuing injury process after hypoxia–ischemia (HI) may progress for days and weeks and is the result of both impaired brain development and continuing destructive processes such as inflammation (2–4). There are indications that exposure to hyperoxia may increase such injury (5).

Oxygen supplementation in postinjury care is used to maintain adequate oxygen saturation in the cardiorespiratory unstable neonate, and exposure to supraphysiological levels of oxygen is often unavoidable. The international guidelines for the immediate resuscitation of term infants was recently changed and currently recommends beginning with room air (21% O₂) rather than hyperoxia (100% O₂) (6) because an increased mortality after hyperoxic resuscitation has been shown in these infants (7). Uncertainty remains for the optimal regimen in preterm infants and later on during postinjury care. There is a need to study both the effect of hyperoxia after an acute hypoxic–ischemic episode and the effect of long-term treatment with oxygen on the development of injury in preterm children.

Repeated multimodal magnetic resonance imaging (MRI) is an excellent tool to study the long-term impact of hyperoxia on the evolution of injury in immature gray and white matter after HI *in vivo*. We have previously shown how areas of delayed tissue loss and ongoing inflammation can be depicted with repeated high-resolution manganese-enhanced T₁ and T₂ images after HI in the 7-d-old (P7) rat (8,9). Additional MRI methods to study the long-term evolution of injury *in vivo* are early diffusion mapping and longitudinal diffusion tensor imaging (DTI) that can be used to detect the long-term changes in water diffusion and thereby the microstructure of developing gray and white matter.

We hypothesized that a single episode of hyperoxia would worsen the long-term trajectory of delayed injury in gray and white matter after HI in the immature rat brain. The aim of the study was to explore this effect up to 42 d after HI using multimodal MRI.

RESULTS

Body weight (**Table 1**) was restricted in all HI animals compared longitudinally with sham. There were no differences between HI groups.

¹Department of Laboratory Medicine, Children's and Women's Health, Norwegian University of Science and Technology (NTNU), Trondheim, Norway; ²Regional Centre for Child and Adolescent Mental Health, Norwegian University of Science and Technology, Trondheim, Norway; ³Department of Circulation and Medical Imaging, Norwegian University of Science and Technology, Trondheim, Norway; ⁴Department of Radiology, St. Olav University Hospital, Central Norway Regional Health Authority, Trondheim, Norway; ⁵Department of Pediatrics, St. Olav University Hospital, Central Norway Regional Health Authority, Trondheim, Norway. Correspondence: Tora Sund Morken (tora.s.morken@ntnu.no)

Received 16 December 2011; accepted 27 September 2012; advance online publication 9 January 2013. doi:10.1038/pr.2012.170

Effects of Hyperoxia on Long-Term Tissue Destruction After HI

On day 1, areas of high T_2 were seen in the ipsilateral hemisphere (Figure 1a). These areas later underwent destruction and impaired growth. HI+hyperoxia had lower ipsilateral hemisphere volumes and larger porencephalic cysts than HI+room air at all time points (Figure 1b,d). There was a significant interaction in the linear mixed model between time and experiment group in ipsilateral hemisphere volume ($P < 0.001$) and porencephalic cyst volume ($P < 0.001$). This was seen as a more severe trajectory of brain tissue destruction with increasing differences in ipsilateral hemisphere and porencephalic

cyst volumes between HI+room air and HI+hyperoxia over the 42-d follow-up period after injury (Figure 1).

Manganese Enhancement and the Inflammatory Response

Increased manganese enhancement was observed in both the HI groups 7 d after HI in ipsilateral basal ganglia, thalamus, and cortex (Figure 2c–e). Areas of activated microglia and reactive astrocytes were seen in the manganese-enhanced areas in both groups. A slightly higher proportion of the ipsilateral brain tissue was manganese enhanced in HI+hyperoxia vs. HI+room air (not significant, $P = 0.066$). Mean CD68 score was higher in HI+hyperoxia than in HI+room air on day 7 after HI ($P = 0.02$; Figure 2b). Mean antigial fibrillary acid protein score and counts of caspase-3-positive cells did not differ between HI+room air and HI+hyperoxia.

Early Apparent Diffusion Coefficient and Long-Term Outcome After HI

Apparent diffusion coefficient (ADC) values were lower in ipsilateral basal ganglia and hippocampus in HI+hyperoxia than in

Table 1. Longitudinal mean body weight \pm SEM

	Day 0 (g)	Day 1 (g)	Day 7 (g)	Day 21 (g)	Day 42 (g)
HI+hyperoxia	15.7 \pm 0.5*	15.6 \pm 0.5*	24.4 \pm 1.1*	60.2 \pm 4.1*	170.5 \pm 8.1
HI+room air	15.1 \pm 0.4	15.1 \pm 0.4*	24.0 \pm 0.6*	65.8 \pm 1.6*	167.3 \pm 5.2
Sham	14.7 \pm 1.1	16.8 \pm 1.1	28.8 \pm 0.7	76.6 \pm 1.9	189.3 \pm 8.2

HI, hypoxia-ischemia.

* $P < 0.05$ vs. sham.

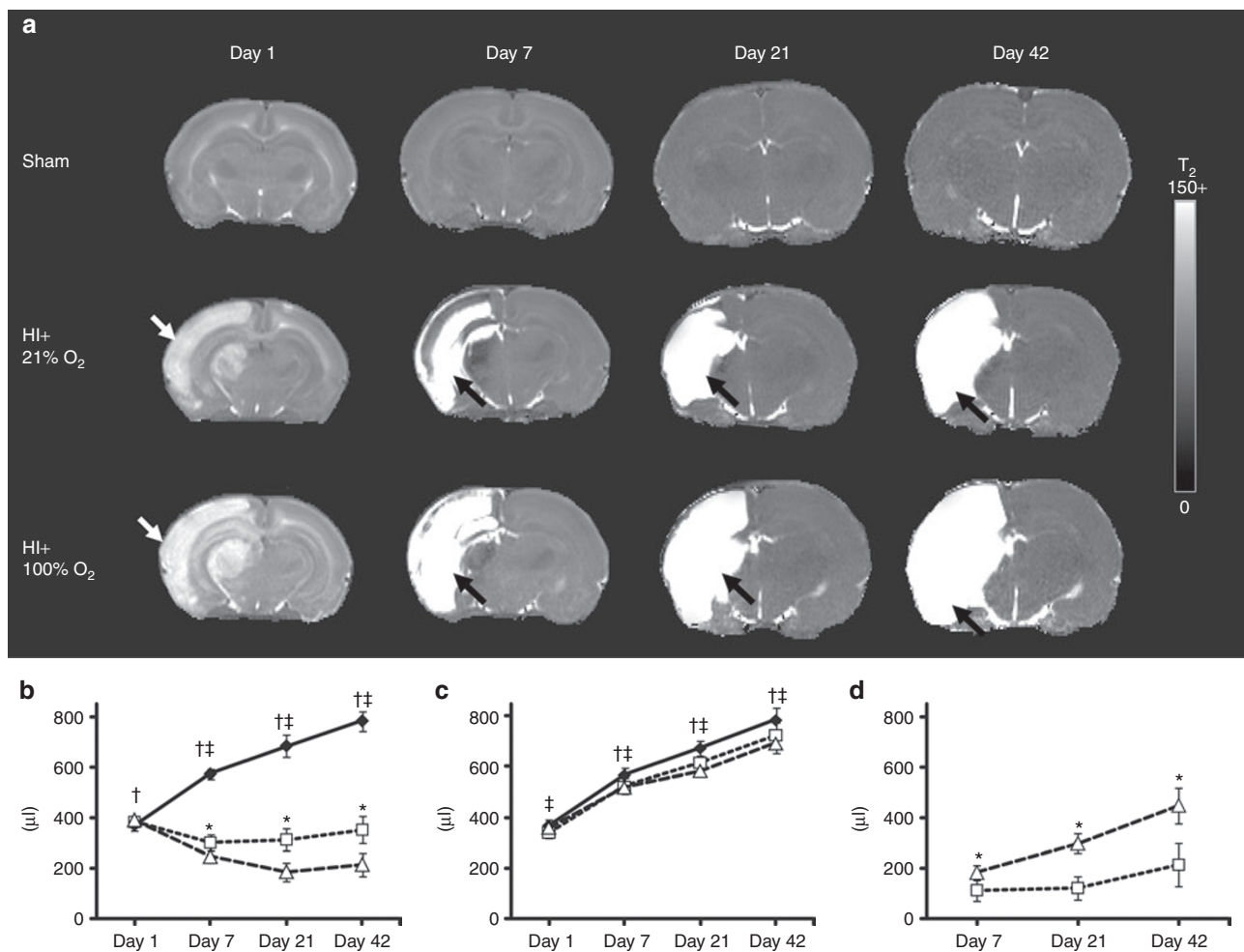


Figure 1. Effects of hyperoxia on long-term tissue destruction after hypoxia-ischemia (HI). (a) T_2 maps; (b) ipsilateral hemisphere volume; (c) contralateral hemisphere volume; and (d) porencephalic cyst volume; all from days 1, 7, 21, and 42 after (HI) in HI+hyperoxia (open triangle), HI+room air (open square), and sham (black diamond). Areas with increased T_2 (white arrows) on day 1 show injured areas with edema. The same area dissolved into a porencephalic cyst seen as high T_2 in liquid areas on days 7, 21, and 42 (black arrows). Bars represent 95% confidence intervals. * $P < 0.05$ HI + hyperoxia vs. HI + room air; † $P < 0.05$ HI + hyperoxia vs. sham; ‡ $P < 0.05$ HI + room air vs. sham.

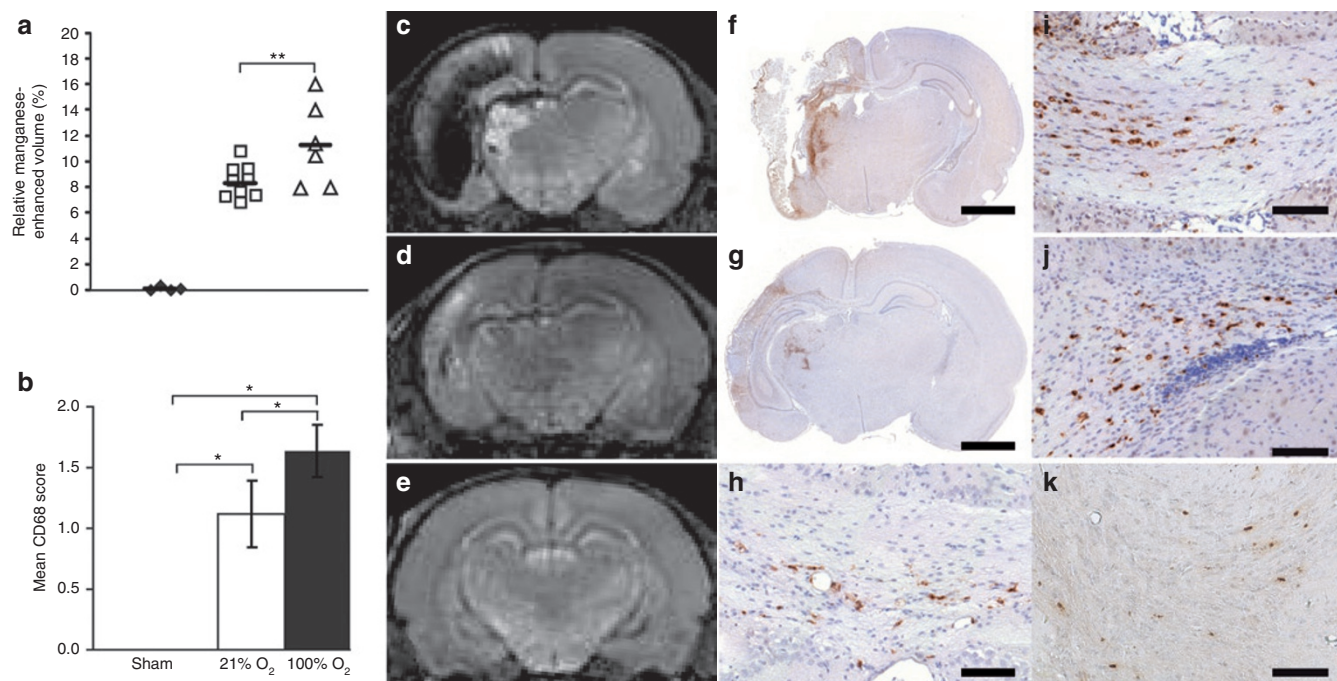


Figure 2. Manganese enhancement and delayed inflammation. (a) Relative manganese-enhanced volume in ipsilateral hemisphere in HI+hyperoxia (open triangle), HI+room air (open square), and sham (black diamond); **not significant, $P = 0.066$. (b) Mean CD68 score in HI+hyperoxia (black column) and HI+room air (white column). Bars represent 95% confidence intervals. * $P < 0.05$. (c–e) T_1 -weighted images with manganese enhancement (bright areas) in (c) HI+hyperoxia, (d) HI+room air, and (e) sham; (f,g) CD68-positive microglial cells (brown) in (f) HI+hyperoxia and (g) HI+room air. In f,g, bars = 2 mm. (h,i) Microglial cells were seen extending into the corpus callosum and (j) contralateral cingulum. Scattered caspase-3-positive cells were seen in contralateral hemisphere in the area of the external capsule (k). In h–k, bars = 100 μm , $\times 20$ magnification. HI, hypoxia–ischemia.

Table 2. Mean ADC ($\text{m}^2/\text{s} \times 10^{-6}$) and 95% CI in ipsilateral basal ganglia, thalamus, hippocampus, and cortex 1 day after HI

	HI+hyperoxia		HI+room air		Sham	
	Mean	95% CI	Mean	95% CI	Mean	95% CI
Basal ganglia	614.5	(545.8–638.1)**	802.6	(679.8–925.5)*	1,105.7	(1,035.0–1,176.4)
Thalamus	611.1	(533.2–689.0)*	795.9	(641.3–950.5)*	1,134.8	(1,093.5–1,176.0)
Hippocampus	767.2	(695.2–839.3)**	912.3	(817.4–1,007.3)*	1,122.4	(1,079.9–1,164.9)
Cortex	456.1	(366.3–545.9)*	649.5	(486.2–812.9)*	1,029.3	(991.8–1,066.8)

ADC, apparent diffusion coefficient; CI, confidence interval; HI, hypoxia–ischemia.

* $P < 0.05$ vs. sham; ** $P < 0.05$ HI+hyperoxia vs. HI+room air and sham.

HI+room air 1 d after HI with the same tendency in thalamus ($P = 0.06$) and cortex ($P = 0.1$), indicating a more severe injury in this group (Table 2). Both HI groups had lower ADC values in all regions vs. sham. ADC on day 1 after HI was positively correlated with long-term ipsilateral hemisphere volumes (Table 3), especially in thalamus. HI+room air had an overall stronger correlation between day 1 ADC and long-term ipsilateral hemisphere volumes than HI+hyperoxia. Visual evaluation of ADC maps 1 d after HI identified four patterns of abnormality that could be related to different trajectories of brain tissue loss (Figure 3a). These were pattern 1: no injury, could not be distinguished from sham ($n = 1$); pattern 2: high ADC and high signal intensity on T_2 maps in external capsule only ($n = 14$); pattern 3: low ADC in cortex, thalamus, and hippocampus ($n = 26$); and pattern 4: ADC change in contralateral hemisphere ($n = 6$). In animals with high ADC and high T_2 in white matter

(pattern 2), the ipsilateral hemisphere had an impaired growth resulting in hypotrophy of the ipsilateral hemisphere without dissolution and cyst development (Figure 3c). This resulted in larger ipsilateral brain hemisphere volumes in the long term than animals with a reduction in ADC in ipsilateral (pattern 3) or contralateral hemisphere (pattern 4). Animals with pattern 3 or 4 had total hemisphere destruction in the long term with a porencephalic cyst occupying most of the ipsilateral area of the brain (Figure 3c).

Diffusion Tensor Imaging in Corpus Callosum and Contralateral White Matter

DTI was performed on day 21 and day 42 after HI. On day 21 after HI, fractional anisotropy (FA) in corpus callosum was lower in HI+hyperoxia than in HI+room air that again was lower than in sham (Figure 4d). From day 21 to day 42, FA increased in

Table 3. Correlations between ADC values on day 1 and ipsilateral hemisphere volume on days 7, 21, and 42

Independent variable	Dependent variable: ipsilateral hemisphere volume								
	Day 7			Day 21			Day 42		
ADC on day 1	Constant	<i>B</i>	<i>R</i> ²	Constant	<i>B</i>	<i>R</i> ²	Constant	<i>B</i>	<i>R</i> ²
Basal ganglia									
HI+hyperoxia	82.4	0.3	0.41*	228.0	-0.1	0.09	161.8	0.1	0.01
HI+room air	91.9	0.3	0.74*	86.9	0.3	0.63*	60.7	0.4	0.70*
Thalamus									
HI+hyperoxia	92.1	0.3	0.47*	-28.3	0.4	0.40*	-82.6	0.5	0.56*
HI+room air	151.2	0.2	0.66*	132.5	0.2	0.8*	122.2	0.3	0.84*
Hippocampus									
HI+hyperoxia	67.0	0.2	0.32*	120.9	0.1	0.05	81.1	0.2	0.17
HI+room air	-24.3	0.4	0.77*	-2.3	0.4	0.69*	-62.9	0.5	0.80*
Cortex									
HI+hyperoxia	172.3	0.2	0.31*	223.4	-0.1	0.02	180.7	0.1	0.02
HI+room air	200.6	0.2	0.56*	217.9	0.2	0.34	213.7	0.2	0.49*

ADC, apparent diffusion coefficient; HI, hypoxia-ischemia.

**P* < 0.05.

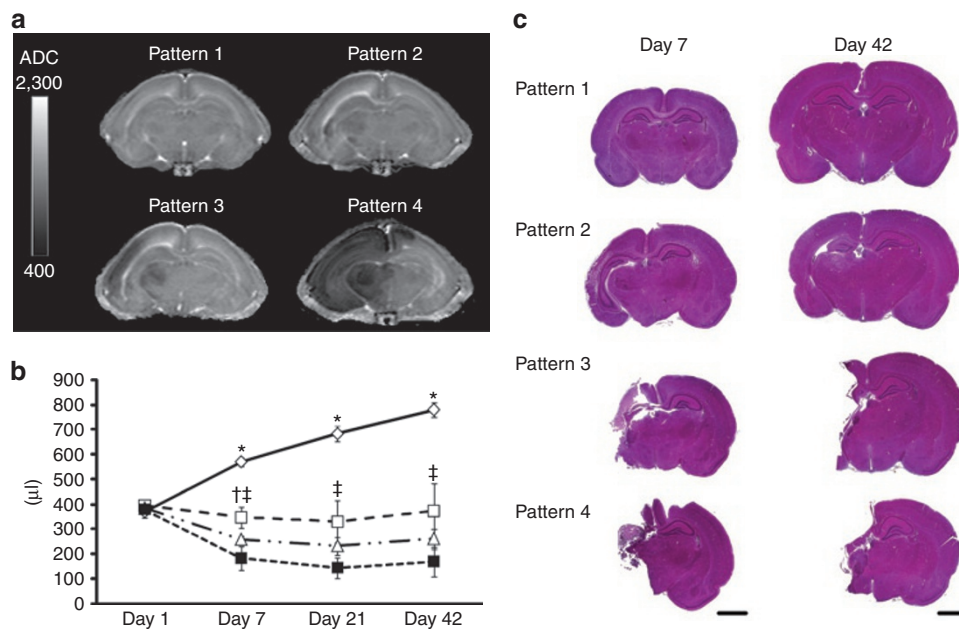


Figure 3. Early apparent diffusion coefficient and long-term outcome after HI. (a) ADC maps 1 d after HI with four different patterns of injury. Pattern 1: no injury and sham; pattern 2: high ADC in external capsule only; pattern 3: low ADC in cortex, thalamus, and hippocampus; pattern 4: ADC changes in contralateral hemisphere. (b) Graph of ipsilateral brain tissue volume from days 1 to 42 in animals from pattern 1 (open diamond), pattern 2 (open square), pattern 3 (open triangle), and pattern 4 (black square). (c) Hematoxylin-eosin-stained slices from days 7 and 42 (scale bar = 2 mm). Group mean with error bars representing 95% confidence intervals. **P* < 0.05 pattern 1 vs. patterns 2-4; †*P* < 0.05 pattern 2 vs. pattern 3; ‡*P* < 0.05 pattern 2 vs. pattern 4. ADC, apparent diffusion coefficient; HI, hypoxia-ischemia.

HI+room air (*P* = 0.004), whereas it remained unchanged in HI+hyperoxia and sham. This resulted in similar values of FA in HI+room air and sham on day 42. The changes in FA were associated with changes in radial diffusivity. On day 21, radial diffusivity was higher in HI+hyperoxia than in HI+room air, and both were higher than in sham. From day 21 to day 42, radial diffusivity decreased in HI+room air (*P* = 0.001) to values similar to sham on day 42, whereas no change was seen in sham

or HI+hyperoxia (Figure 4e). Axial diffusivity did not differ between experiment groups on either time point but increased in HI+hyperoxia from day 21 to day 42. There was a significant interaction between time and experiment group in radial and axial diffusivity (*P* = 0.03).

In contralateral white matter, FA did not differ between experiment groups or time points, but there was a tendency toward higher axial (*P* = 0.05) and radial (*P* = 0.09) diffusivity in HI+hyperoxia

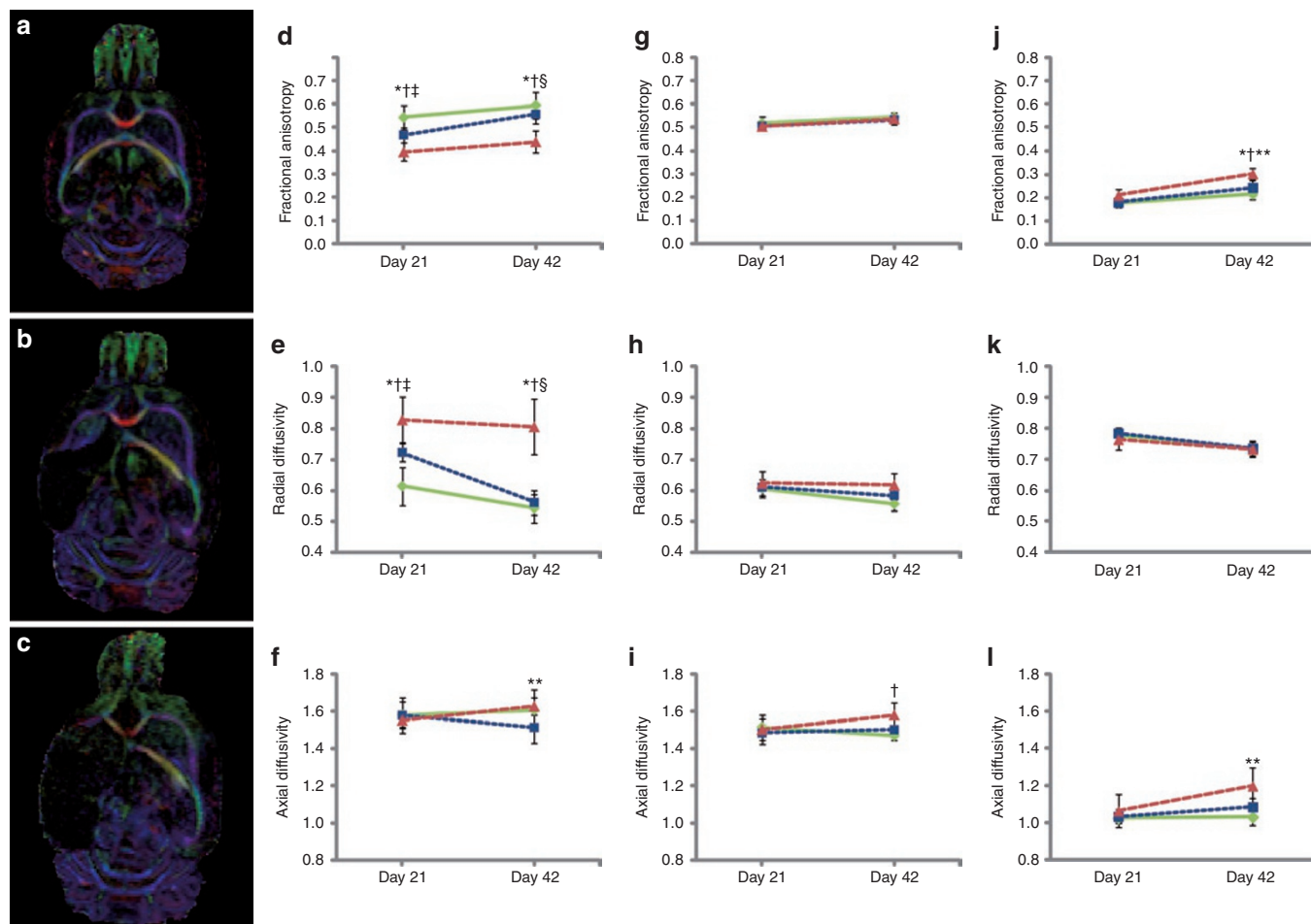


Figure 4. Diffusion tensor imaging. (a–c) Directionally color-coded fractional anisotropy maps from day 42 after hypoxia–ischemia (HI) in sham (a), HI+room air pup with mild injury (b), and HI+hyperoxia pup with severe injury (c). (d–f) Fractional anisotropy (d), radial diffusivity (e), and axial diffusivity (f) in corpus callosum. (g–i) Fractional anisotropy (g), radial diffusivity (h), and axial diffusivity (i) in contralateral white matter. (j–l) Fractional anisotropy (j), radial diffusivity (k), and axial diffusivity (l) in contralateral putamen. All diffusion tensor imaging metrics are from days 21 and 42 after HI and show HI+hyperoxia (red triangle), HI+room air (blue square), and sham (green triangle). Graphs show means and 95% confidence intervals for each group. * $P < 0.05$ HI+hyperoxia vs. HI+room air; † $P \leq 0.05$ HI+hyperoxia vs. sham; ‡ $P < 0.05$ HI+room air vs. sham; § $P < 0.05$ HI+room air day 21 vs. day 42; ** $P \leq 0.05$ HI+hyperoxia day 21 vs. day 42.

vs. sham on day 42 (Figure 4h–i). In contralateral caudate putamen, FA and axial diffusivity in HI+hyperoxia increased from day 21 to day 42, and FA was higher in HI+hyperoxia vs. HI+room air and sham on day 42 (Figure 4j–l).

Changes in Contralateral Hemisphere

T_2 values were evaluated in the contralateral hemisphere but did not differ between experiment groups (data not shown). ADC values were lower in contralateral parasagittal cortex in HI+hyperoxia than in HI+room air and sham ($P < 0.05$) and were positively correlated with low contralateral hemisphere volumes on day 42 ($R^2 = 0.59$; $P = 0.003$). Growth of the contralateral hemisphere was restricted in all HI animals compared longitudinally with sham, with no differences between HI groups (Figure 1c). There was a positive correlation between body weight and contralateral hemisphere volume on day 42 ($R^2 = 0.62$; $P < 0.001$). On immunohistochemistry on day 7 after HI, activated microglial cells were observed in either corpus callosum or contralateral cingulum in 86% of HI+hyperoxia

and 81% of HI+room air, and scattered apoptotic cells were observed in contralateral hemisphere in both the HI groups (Figure 2h–k).

DISCUSSION

Exposure to hyperoxia after HI in the P7 rat induced a more severe initial brain injury with increased tissue loss during the subsequent weeks as compared with exposure to room air. The larger tissue destruction associated with hyperoxia after HI was accompanied by signs of increased inflammation. The severity of late injury correlated with the reduction in ADC in brain tissue on day 1 after HI and depended on whether ADC was abnormal in white matter only or in both gray and white matter on day 1. DTI metrics indicated irreversible changes in white matter microstructure in corpus callosum after HI and hyperoxia. Hyperoxia also seemed to have a detrimental effect on white matter development in the contralateral hemisphere and an influence on long-term brain growth.

Strengths and Limitations

The strength of this study is the detailed information about brain development and injury obtained by multimodal MRI follow-up *in vivo* combined with immunohistochemistry. To our knowledge, it is the first study to examine the effect of hyperoxia after HI on long-term injury development in gray and white matter in a neonatal rat model using manganese-enhanced MRI in combination with DTI and anatomical imaging. Although some experimental studies have found no effect (10) or that hyperoxia limits injury (11), mounting experimental data indicate that hyperoxia exacerbates injury after HI in the immature brain (5,12). Our study corroborates these findings and adds important knowledge to the effect of hyperoxia on the prolonged evolution of injury in gray and white matter. Two hours of hyperoxia was used to demonstrate an effect on the trajectories of gray and white matter injury development. However, this does not translate directly to a clinical setting, in which exposure is typically repeated, shorter, and fluctuating between low and high oxygen concentrations. A possible limitation is that whole litters were used. To appropriately analyze this design, we applied a mixed model that recognizes that litters, not individual pups, were assigned to the experiment groups. This model takes into account the random effects of litters (clusters) when measuring the fixed effects of experiment groups.

Comparative Aspects of the P7 Rat Model

The Vannucci model in the P7 rat has often been considered a late-preterm model because the cortical layering is complete (13), but myelination of white matter has not yet started (14). Such a comparison between the human and rodent brain will always be arbitrary because of the differences in brain development and anatomy between these species. In human brain development, most neural events occur before birth, whereas in the rat, many of these events occur after birth (15). Also, the rat brain has a lissencephalic surface, whereas the human brain is gyrencephalic.

Long-Term Tissue Destruction

Exposure to hyperoxia after HI led to more severe longitudinal tissue destruction as demonstrated by the more pronounced brain tissue loss and larger porencephalic cysts in HI+hyperoxia than in HI+room air. In this and earlier studies, we have shown that areas of manganese enhancement 7 d after HI correspond to areas of inflammation and gliosis that later undergo delayed cell death and liquefaction, suggesting that inflammation is involved in the continued destruction of brain tissue after HI (8,9). The indications of a stronger inflammatory response in HI+hyperoxia in our study are in agreement with earlier animal studies reporting that inflammation in the perinatal brain (16) and activated microglia in the adult brain (17) increase after hyperoxic reperfusion. A more pronounced delayed inflammatory response may either have been caused by larger areas of initial injury in animals exposed to hyperoxia after HI or by a direct enhancing effect of hyperoxia on inflammation.

Early ADC and Long-Term Outcome

Early ADC changes observed in gray matter in HI+hyperoxia could be explained by a more severe cytotoxic edema causing restriction of water movement due to cellular swelling and reduction of extracellular space (18). This is in accordance with current knowledge of increased oxidative stress in the reperfusion phase leading to increased cellular injury (19), possibly potentiated by a vasoconstricting effect of hyperoxia after injury (20). ADC is used in the clinic for early assessment of perinatal brain injury because diffusion abnormalities appear earlier than signal abnormalities on T_2 and T_1 imaging. The finding that early low ADC in thalamus correlated with lower ipsilateral hemisphere volume longitudinally is in agreement with human studies in which low early ADC in this area predicted long-term MRI injury patterns and neurologic outcome after HI (21,22). The correlation was strongest in HI+room air, possibly explained by a more homogenous severe destruction of brain tissue in the HI+hyperoxia group in the long term. Our findings of high ADC in white matter in injury pattern 2 have been reported in animal studies as a sign of subtle white matter injury after HI (23) and also in studies of preterm infants with white matter diffuse excessive high signal intensity at term-equivalent age (24). High ADC indicates the presence of free extracellular water, supported by high T_2 observed in white matter in the same animals. One possible explanation is vasogenic edema extending into white matter from adjacent injured areas. Other possible explanations are cellular reactions in oligodendrocytes and microglia in white matter (25), and apoptosis causing cellular shrinkage and increase in extracellular space (26,27).

DTI

Lower FA and increased radial diffusivity in corpus callosum in HI+hyperoxia in our study may indicate pathological changes in white matter microstructure. White matter deviations are often seen in preterm infants (28), and both hypoxia and ischemia, as well as hyperoxia, are thought to play an important role in the pathogenesis (4,29). During normal maturational development of white matter in rats, increasing FA and decreasing radial diffusivity observed during the first postnatal weeks are thought to be related to increasing oligodendrocyte coverage and myelination of white matter tracts (30,31). One may speculate whether reduced myelination or axonal injury and loss of transcallosal fibers may have contributed to the lower FA and increased radial diffusivity. The normalization of DTI metrics from day 21 to day 42 in HI+room air may indicate repair. In contrast, this normalization was not seen among HI+hyperoxia, possibly indicating an irreversible effect of hyperoxia on immature white matter. This is in agreement with emerging evidence of selective vulnerability of white matter to prolonged hyperoxia exposure during the first postnatal week in rats (29), leading to long-term reduction in FA of corpus callosum (32). The observation of activated microglia in white matter supports the hypothesis that these cells, abundant in developing white matter, are key effectors in the pathogenesis of injury to perinatal white matter (4).

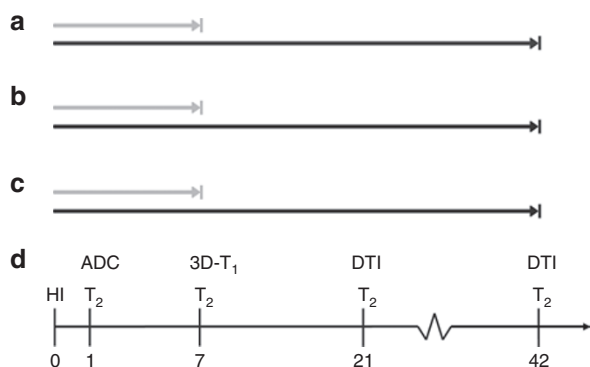


Figure 5. Experimental design with experiment groups. (a) HI+hyperoxia, (b) HI+room air, (c) sham, and (d) timeline of days after HI with respective MRI modalities. Animals were followed with repeated MRI for either 7 d after HI (gray arrows) (in **a**, $n = 15$; in **b**, $n = 9$; and in **c**, $n = 6$) or for 42 d after HI (black arrows) (in **a**, $n = 13$; in **b**, $n = 10$; and in **c**, $n = 7$). HI, hypoxia-ischemia; MRI, magnetic resonance imaging.

Our observations of DTI abnormalities in contralateral white matter and caudate putamen have correlates in clinical studies. In preterm infants with diffuse excessive high signal intensity in white matter indicating white matter abnormality, increased axial and radial diffusivity have been found on DTI (33). DTI studies of normal aging subjects have revealed higher FA and axial diffusivity in basal ganglia attributed to tissue degradation and a relatively more compact tissue (34). A restricted volume of basal ganglia has been shown in preterm infants (35), parallel to our findings of lower contralateral brain volume after HI in the long term. One may speculate that a similar process of relative tissue degradation and restricted growth in the developing brain after perinatal HI has led to the observed changes in DTI metrics in caudate putamen in our study.

Contralateral Hemisphere

Signs of injury in the contralateral hemisphere may have been caused by the global hypoxia in this model of HI. Restricted contralateral hemispheric growth has also been reported by others (36,37), and observations of activated microglia and scattered apoptotic cells suggest that delayed injury processes are activated. A potentiating effect of hyperoxia in the reperfusion phase is also possible. Vasoconstriction by hyperoxia has earlier been reported in the reperfusion phase in preterm infants (20) and may have worsened the injury and the subsequent cytotoxic edema in areas of immature vascularization in the developing brain; in our study seen as a reduction in ADC in contralateral parasagittal cortex in HI+hyperoxia 1 day after HI.

Conclusion

Exposure to hyperoxia after HI caused adverse effects in gray and white matter development that increased during the course of the longitudinal study. The evolving tissue destruction and loss of white matter integrity may have been caused by increased inflammatory reactions, either as a direct consequence of hyperoxia or indirectly through a more severe initial injury. Our study corroborates the emerging evidence of vulnerability to hyperoxia of immature gray and white matter and adds important

knowledge to the impact of hyperoxia on long-term development of injury. We suggest that future studies should examine the effects of fluctuating oxygen concentrations on circulation and development of gray and white matter in the immature brain to better mimic the clinical conditions of the preterm neonate.

METHODS

Animals

Animals were obtained from Scanbur, Norway AS. Six Wistar rats, mated at the animal facility at the Norwegian University of Science and Technology in Trondheim, gave birth to litters of 9–14 pups. The pups ($n = 60$) were weaned at the age of 4 wk (P28) and kept on a 12:12 h light:dark cycle with food and water *ad libitum*. Experiments were approved by the Animal Care and Use Committee at the Norwegian University of Science and Technology (Forsøksdyrvalget).

HI and Experiment Groups

The Vannucci model for HI brain injury was used (9,14). P7 rats were placed on a water-heated thermal pad (Gaymar Industries, Orchard Park, NY) and anesthetized with isoflurane (Baxter, Allerød, Denmark). The right common carotid artery was identified, thermocauterized, and severed. In sham-operated littermates, the carotid artery was identified under anesthesia but not severed ($n = 13$). The pups were returned to their dam for recovery and feeding for a minimum of 2 h and a maximum of 4 h. Thereafter, the pups were put in a fiberglass box inside an incubator, where the temperature and oxygen concentrations were constantly monitored and the temperature was kept at $36 \pm 0.5^\circ\text{C}$. The box was flushed with preheated, humidified 8% O₂ in 92% N₂, and the oxygen concentration was kept constant for 75 min. Immediately after hypoxia, the box was flushed with either 100% O₂ or room air. After saturating the box with the desired gas concentration, flow was kept at a minimum during exposure. Four litters ($n = 28$) were exposed to 100% O₂ (HI+hyperoxia), and two litters ($n = 19$) were exposed to room air (HI+room air) for 2 h. More pups were allocated to the HI+hyperoxia group because a larger injury variability was expected in this group.

Manganese Enhancement

For manganese-enhanced MRI, MnCl₂ (Sigma-Aldrich, St Louis, MO) was given as a single dose (40 mg/kg body weight) by intraperitoneal injection 6 h after hypoxia (one litter from each experiment group and sham-operated littermates; $n = 20$). The animals that did not receive MnCl₂ were injected with 0.15 ml of 0.9% NaCl (B. Braun Melsungen, Germany; $n = 40$).

MRI

MRI was performed on days 1, 7, 21, and 42 after HI using a 7-Tesla magnet (Biospec 70/20 AS; Bruker Biospin MRI, Ettlingen, Germany) with water-cooled (BGA-12, 400 mT/m) gradients. A volume resonator (Bruker Biospin MRI) was used for radio frequency transmission, and actively decoupled head surface coils (Rapid Biomedical, Rimpar, Germany) were used for radio frequency reception. During scanning, the anesthetized (2% isoflurane in 30% O₂/70% N₂) pups lay prone in a dedicated water-heated bed (Bruker Biospin MRI), and the heads were fixated in the same position with tooth bar, nose mask, and polystyrene. Temperature and respiration were monitored during the scanning procedure. All animals were imaged longitudinally at all time points until euthanization (Figure 5). On day 1, diffusion-weighted images were obtained using an echo planar imaging sequence with six b values (100/200/400/600/800/1,000 ms) in three orthogonal directions; echo time (TE) = 37.50 ms; repetition time (TR) = 3,000 ms; four averages; field-of-view (FOV) = $25 \times 30 \text{ mm}^2$; acquisition matrix (MTX) = 160×192 ; 15 coronal slices of 1 mm. On day 7, three-dimensional T₁-weighted data sets were obtained using a gradient echo fast low-angle shot sequence with flip-angle = 30° ; TR = 12 ms; TE = 3.0 ms; FOV = $25 \times 25 \times 17.5 \text{ mm}^3$, and MTX = $160 \times 160 \times 112$. Two-dimensional coronal T₂ maps were obtained at all time points with a turbo spin-echo (RARE) sequence: Effective TE = 25, 75, and 125 ms; TR = 4,000 ms; RARE-factor = 4; FOV = $25 \times 20 \text{ mm}^2$ (day 1 and day 7), $30 \times 20 \text{ mm}^2$ (day 21 and day 42); MTX = 160×96 (day 1 and day 7), and 192×96 (day 21 and day 42) reconstructed to 160×128 and 192×128 ,

respectively; 15 slices of 1 mm. On days 21 and 42, DTI was performed with an echo planar imaging sequence using 30 directions; $b = 1,000$ ms; five b_0 images; TE = 40 ms; TR = 3,750 ms; FOV = 40×49.5 mm²; MTX = 172×212 ; 25 axial slices of 0.5 mm.

Magnetic Resonance Image Analyses

Gray matter changes were studied by ADC maps from day 1 after HI and by manganese-enhanced three-dimensional T_1 imaging from day 7 after HI. Volume measurements of the injured brain areas were carried out on T_2 maps at all time points along with the assessment of the anatomical distribution of injury. The long-term white matter development was studied by DTI on day 21 and day 42 after HI. In-house-developed software (MATLAB version R2010a, Math Works, Natick, MA) was used for calculating the ADC and T_2 maps, and ImageJ (v1.42q, National Institutes of Health, Bethesda, MD) was used for image analyses. The ADC maps were calculated by fitting a monoexponential model to the signal intensity of the images with different b values. Regions of interest were drawn in parasagittal cortex, thalamus, hippocampus, and basal ganglia in one slice corresponding to -3.25 mm from the bregma (38). The T_2 maps were calculated by fitting a monoexponential model to the signal intensity of the images with different TE values. The area of the remaining brain tissue in each hemisphere and porencephalic cysts were drawn manually on the T_2 maps in each image slice, and the total volumes were calculated. Manganese-enhanced areas in the ipsilateral hemisphere were defined by having higher signal intensity on T_1 -weighted images than on the contralateral side on day 7 (8). Areas of manganese-enhanced tissue were manually drawn in each image slice, and the manganese-enhanced volumes calculated. DTI analyses were performed with the tools of the FMRIB software library (FSL version 4.1.4, Oxford Centre for Functional MRI of the Brain, Oxford, UK; www.fmrib.ox.ac.uk/fsl). Images were preprocessed to reduce image artifacts due to motion and eddy current distortions by affine transformation and coregistration of the diffusion-encoded images to the b_0 images. Single data sets with severe ghosting artifacts were excluded from further analyses (day 21: $n = 6$; day 42: $n = 5$). Brains were segmented out using the Brain Extraction Tool before FDT version 2.0 (both part of FSL) was used to fit a voxelwise diffusion tensor model to the diffusion image data (39). Maps for the FA, radial diffusivity, and axial diffusivity were created. To limit partial volume effects, regions of interest were manually drawn in the center of white matter structures at all relevant image slices on the FA maps and combined to three volumes of interest that were used in the analyses: corpus callosum (comprising the genu, body, and splenium), contralateral major white matter structures, and contralateral caudate putamen. Mean FA, radial diffusivity, and axial diffusivity were calculated in each of these volumes of interest in each animal. Due to severe tissue loss, regions of interest were not drawn in ipsilateral white matter.

Immunohistochemistry

Animals were killed after MRI acquisition on day 7 or 42 by an overdose of pentobarbital (300 mg/kg; Vétoquinol, Lure, France). For fixation, an intracardial perfusion of 4% paraformaldehyde (Fluka Chemie AG, Buchs, Switzerland) in phosphate-buffered saline (Oxoid Limited, Hampshire, UK) was given. After embedding in paraffin, coronal sections (8 μ m) corresponding to -3.25 mm from the bregma (38) were cut and stained with hematoxylin–eosin (Cell Path, Newtown, UK and Sigma-Aldrich), antiED1–fluorescein isothiocyanate (Serotec, Raleigh, NC) for CD68-positive microglia, antigial fibrillary acid protein (Cybus Biotechnology, Southampton, UK) for reactive astrocytes, or anticlaved-caspase-3 (Cell Signaling, Danvers, MA) for apoptosis. The sections were then incubated with rat antifluorescein isothiocyanate–biotin (Roche, Basel, Switzerland), horse antimouse–biotin (Vector Laboratories, Burlingame, CA), or goat antirabbit–biotin (Vector Laboratories). Visualization was performed using a Vectastain ABC kit (Vector Laboratories). The sections were evaluated semiquantitatively for the presence of CD68 or antigial fibrillary acid protein–positive cells in 13 defined regions: parietal cortex divided into six subregions, CA1, CA2, CA3, CA4, dentate gyrus, thalamus, and caudate putamen (10). The following scale was used for scoring: 0, no positive cells; 1, <33% of cells in area stained; 2, 33–67% stained;

3, >67% stained. The average of the scored regions was defined as the mean score. For regions in total dissolution, no score was given. Caspase-3 immunoreactive cells were counted in ipsi- and contralateral hemisphere. Full-section images were captured with a MIRAX MIDI system (Carl Zeiss MicroImaging, Jena, Germany). On day 42, semiquantitative analyses were not performed because of large areas of destruction in the ipsilateral hemisphere.

Statistical Analyses

Data were analyzed at each time point using a linear mixed model with experiment group as fixed effect and litter as random effect and are presented as estimated marginal means with 95% confidence intervals unless stated otherwise. Time trajectories of the HI+hyperoxia vs. HI+room air groups were compared using a mixed model with group and categorized time as fixed effects, individual as level 2 random effect, and litter as level 3 random effect, using a likelihood ratio test for the time \times group interaction. Analyses of the DTI metrics between time points were performed by paired Student's t -test, and therefore subjects with missing DTI data at either time point were excluded. ADC, immunohistochemistry, and manganese-enhancement data were not normally distributed and were analyzed with Mann–Whitney U -test. A two-sided P value of < 0.05 was considered significant. Analyses were performed in Stata 10 (StataCorp, College Station, TX) and SPSS 16 (SPSS, Chicago, IL).

ACKNOWLEDGMENTS

The authors thank the FUGE Molecular Imaging Center for technical support and Tina Bugge-Pedersen for expert technical assistance.

STATEMENT OF FINANCIAL SUPPORT

This work was supported by a grant from the Liaison Committee between the Central Norway Regional Health Authority and the Norwegian University of Science and Technology (NTNU) (to T.S.M.) and from the Medical Faculty at the Norwegian University of Science and Technology (to M.W.).

REFERENCES

1. Stoll BJ, Hansen NI, Bell EF, et al.; Eunice Kennedy Shriver National Institute of Child Health and Human Development Neonatal Research Network. Neonatal outcomes of extremely preterm infants from the NICHD Neonatal Research Network. *Pediatrics* 2010;126:443–56.
2. Ferriero DM. Neonatal brain injury. *N Engl J Med* 2004;351:1985–95.
3. Geddes R, Vannucci RC, Vannucci SJ. Delayed cerebral atrophy following moderate hypoxia-ischemia in the immature rat. *Dev Neurosci* 2001;23:180–5.
4. Volpe JJ. Brain injury in premature infants: a complex amalgam of destructive and developmental disturbances. *Lancet Neurol* 2009;8:110–24.
5. Koch JD, Miles DK, Gilley JA, Yang CP, Kernie SG. Brief exposure to hyperoxia depletes the glial progenitor pool and impairs functional recovery after hypoxic-ischemic brain injury. *J Cereb Blood Flow Metab* 2008;28:1294–306.
6. Perlman JM, Wyllie J, Kattwinkel J, et al.; Neonatal Resuscitation Chapter Collaborators. Neonatal resuscitation: 2010 International Consensus on Cardiopulmonary Resuscitation and Emergency Cardiovascular Care Science with Treatment Recommendations. *Pediatrics* 2010;126:e1319–44.
7. Saugstad OD, Ramji S, Soll RF, Vento M. Resuscitation of newborn infants with 21% or 100% oxygen: an updated systematic review and meta-analysis. *Neonatology* 2008;94:176–82.
8. Widerøe M, Brekken C, Kavelaars A, et al. Longitudinal manganese-enhanced magnetic resonance imaging of delayed brain damage after hypoxic-ischemic injury in the neonatal rat. *Neonatology* 2011;100:363–72.
9. Widerøe M, Olsen Ø, Pedersen TB, et al. Manganese-enhanced magnetic resonance imaging of hypoxic-ischemic brain injury in the neonatal rat. *Neuroimage* 2009;45:880–90.
10. Grafe MR, Woodworth KN, Noppens K, Perez-Polo JR. Long-term histological outcome after post-hypoxic treatment with 100% or 40% oxygen in a model of perinatal hypoxic-ischemic brain injury. *Int J Dev Neurosci* 2008;26:119–24.

11. Calvert JW, Zhang JH. Oxygen treatment restores energy status following experimental neonatal hypoxia-ischemia. *Pediatr Crit Care Med* 2007;8:165–73.
12. Niatetskaya ZV, Charlagorla P, Matsukevich DA, et al. Mild hypoxemia during initial reperfusion alleviates the severity of secondary energy failure and protects brain in neonatal mice with hypoxic-ischemic injury. *J Cereb Blood Flow Metab* 2012;32:232–41.
13. Eayrs JT, Goodhead B. Postnatal development of the cerebral cortex in the rat. *J Anat* 1959;93:385–402.
14. Rice JE 3rd, Vannucci RC, Brierley JB. The influence of immaturity on hypoxic-ischemic brain damage in the rat. *Ann Neurol* 1981;9:131–41.
15. Yager JY, Ashwal S. Animal models of perinatal hypoxic-ischemic brain damage. *Pediatr Neurol* 2009;40:156–67.
16. Markus T, Hansson S, Amer-Wählin I, Hellström-Westas L, Saugstad OD, Ley D. Cerebral inflammatory response after fetal asphyxia and hyperoxic resuscitation in newborn sheep. *Pediatr Res* 2007;62:71–7.
17. Hazelton JL, Balan I, Elmer GI, et al. Hyperoxic reperfusion after global cerebral ischemia promotes inflammation and long-term hippocampal neuronal death. *J Neurotrauma* 2010;27:753–62.
18. Gass A, Niendorf T, Hirsch JG. Acute and chronic changes of the apparent diffusion coefficient in neurological disorders—biophysical mechanisms and possible underlying histopathology. *J Neurol Sci* 2001;186 Suppl 1: S15–23.
19. Vento M, Asensi M, Sastre J, García-Sala F, Pallardó FV, Viña J. Resuscitation with room air instead of 100% oxygen prevents oxidative stress in moderately asphyxiated term neonates. *Pediatrics* 2001;107:642–7.
20. Lundström KE, Pryds O, Greisen G. Oxygen at birth and prolonged cerebral vasoconstriction in preterm infants. *Arch Dis Child Fetal Neonatal Ed* 1995;73:F81–6.
21. Boichot C, Walker PM, Durand C, et al. Term neonate prognoses after perinatal asphyxia: contributions of MR imaging, MR spectroscopy, relaxation times, and apparent diffusion coefficients. *Radiology* 2006;239:839–48.
22. Rutherford M, Counsell S, Allsop J, et al. Diffusion-weighted magnetic resonance imaging in term perinatal brain injury: a comparison with site of lesion and time from birth. *Pediatrics* 2004;114:1004–14.
23. Meng S, Qiao M, Scobie K, Tomanek B, Tuor UI. Evolution of magnetic resonance imaging changes associated with cerebral hypoxia-ischemia and a relatively selective white matter injury in neonatal rats. *Pediatr Res* 2006;59(4 Pt 1):554–9.
24. Counsell SJ, Allsop JM, Harrison MC, et al. Diffusion-weighted imaging of the brain in preterm infants with focal and diffuse white matter abnormality. *Pediatrics* 2003;112(1 Pt 1):1–7.
25. Lodygensky GA, West T, Moravec MD, et al. Diffusion characteristics associated with neuronal injury and glial activation following hypoxia-ischemia in the immature brain. *Magn Reson Med* 2011;66:839–45.
26. Brauer M. *In vivo* monitoring of apoptosis. *Prog Neuropsychopharmacol Biol Psychiatry* 2003;27:323–31.
27. Wendland MF, Faustino J, West T, Manabat C, Holtzman DM, Vexler ZS. Early diffusion-weighted MRI as a predictor of caspase-3 activation after hypoxic-ischemic insult in neonatal rodents. *Stroke* 2008;39:1862–8.
28. Inder TE, Wells SJ, Mogridge NB, Spencer C, Volpe JJ. Defining the nature of the cerebral abnormalities in the premature infant: a qualitative magnetic resonance imaging study. *J Pediatr* 2003;143:171–9.
29. Gerstner B, DeSilva TM, Genz K, et al. Hyperoxia causes maturation-dependent cell death in the developing white matter. *J Neurosci* 2008;28:1236–45.
30. Bockhorst KH, Narayana PA, Liu R, et al. Early postnatal development of rat brain: *in vivo* diffusion tensor imaging. *J Neurosci Res* 2008;86: 1520–8.
31. Mori S, Zhang J. Principles of diffusion tensor imaging and its applications to basic neuroscience research. *Neuron* 2006;51:527–39.
32. Schmitz T, Ritter J, Mueller S, Felderhoff-Mueser U, Chew LJ, Gallo V. Cellular changes underlying hyperoxia-induced delay of white matter development. *J Neurosci* 2011;31:4327–44.
33. Counsell SJ, Shen Y, Boardman JP, et al. Axial and radial diffusivity in preterm infants who have diffuse white matter changes on magnetic resonance imaging at term-equivalent age. *Pediatrics* 2006;117:376–86.
34. Pfefferbaum A, Adalsteinsson E, Rohlfing T, Sullivan EV. Diffusion tensor imaging of deep gray matter brain structures: effects of age and iron concentration. *Neurobiol Aging* 2010;31:482–93.
35. Peterson BS, Vohr B, Staib LH, et al. Regional brain volume abnormalities and long-term cognitive outcome in preterm infants. *JAMA* 2000;284:1939–47.
36. Andiné P, Thordstein M, Kjellmer I, et al. Evaluation of brain damage in a rat model of neonatal hypoxic-ischemia. *J Neurosci Methods* 1990;35:253–60.
37. Ten VS, Wu EX, Tang H, et al. Late measures of brain injury after neonatal hypoxia-ischemia in mice. *Stroke* 2004;35:2183–8.
38. Paxinos G, Watson C. *The Rat Brain in Stereotaxic Coordinates*, 6th edn. London, UK: Academic Press 2008.
39. Behrens TE, Woolrich MW, Jenkinson M, et al. Characterization and propagation of uncertainty in diffusion-weighted MR imaging. *Magn Reson Med* 2003;50:1077–88.